Nonsegmented PSpice Circuit Model of GaN HEMT With Simulation Convergence Consideration

Hong Li, *Member, IEEE*, Xingran Zhao, Wenzhe Su, Kai Sun, *Senior Member, IEEE*, Trillion Q. Zheng, *Senior Member, IEEE*, and Xiaojie You, *Member, IEEE*

***Abstract*—To solve the simulation convergence problem of enhancement mode gallium nitride high-electron mobility transistor (GaN HEMT) models, this paper proposes a nonsegmented model for GaN HEMT, which uses nonsegmented, smooth continuous equations to describe the static and dynamic characteristics of GaN HEMT. Furthermore, the static characteristic of GaN HEMT obtained by the nonsegmented model is verified by comparing the simulation curves with the static curves provided in datasheet; and the dynamic characteristic obtained by the nonsegmented model is verified by comparing the simulation result with the experimental result based on double pulse test platform. Moreover, to prove the good performance on simulation convergence of the proposed nonsegmented GaN HEMT model, the full-bridge dc–ac converter with four GaN HEMTs has been employed as an example; the simulation result shows the good convergence of the inverter compared to the conventional segmented GaN HEMT model, which make it possible and flexible to research the power converters with GaN HEMTs by simulation way.**

***Index Terms*—Double pulse circuit, gallium nitride high-electron mobility transistor (GaN HEMT), nonsegmented equation, PSpice circuit model, simulation convergence.**

I. Introduction

DUE to the limitations of silicon (Si) material properties, Si-based power electronics semiconductor devices have been gradually unable to meet today's high performance requirements for semiconductor devices in power electronics [1]. Based on this, gallium nitride (GaN) as the representative of the wide band gap semiconductor material came into being, compared to Si devices, GaN has higher bandwidth, breakdown voltage, and thermal conductivity, and these excellent features make GaN have significant advantage in high frequency and high power density applications [2]–[4]. As the most promising switching devices, there are already efficient power conversion corporation (EPC), Transphorm, GaN systems, and other manufacturers to produce GaN high electron mobility transistor (HEMT). In order to predict the characteristics of GaN HEMT and optimize the power electronics circuits design with GaN HEMTs, an accurate GaN HEMT model is necessary [5], [6].

Up to now, the available models of GaN HEMT can be divided into four categories: numerical model, physics-based model, semiphysics-based model, and behavioral model [7], [8]. Numerical model is based on numerical simulation tools (SILVACO, Sentaurus TCAD, etc.), which is quite complicated and the detailed information about material properties and internal structure of GaN HEMT is also required [9], [10]. The physics-based model is based on the physical structure and internal parameters of GaN HEMT, which is very accurate, however, not suitable for power electronics circuit simulations due to the complicated physical parameter extraction process, as well as the long simulation time [11], [12]. Semiphysics-based model is partly based on the physical structure and internal parameters of GaN HEMT, and some behavioral equations are included in the model [13], [14]. Behavioral model is mainly based on behavioral equations of GaN HEMT, the information about the physical structure and the internal parameters of GaN HEMT is not necessary any more [15], [16]. For power electronics circuit simulation, numerical model, physics-based model, and semiphysics-based model are complex and unpractical, since the exact information about material properties, physical structure, and internal parameters of GaN HEMTs are needed. However, the above-mentioned information is very sensitive and it is difficult to obtain for researchers or engineers. Therefore, behavioral model is a good choice for power electronics circuit simulation.

The behavioral models established in [15] and [16] use segmented mathematical equations to describe the static characteristic of GaN HEMT; the equations are divided into three segments according to cutoff region, linear region, and saturation region. But, the behavioral model of GaN HEMTs with segmented equations suffers from the simulation convergence

Manuscript received November 30, 2016; revised March 16, 2017 and May 17, 2017; accepted June 15, 2017. Date of publication July 11, 2017; date of current version October 9, 2017. This work was supported in part by the General Program of the National Natural Science Foundation of China under Grant 51577010 and in part by the National Key Research and Development Program of China under Grant 2016YFE0131700. *(Corresponding author: Hong Li.)*

H. Li, X. Zhao, W. Su, T. Q. Zheng, and X. You are with the School of Electrical Engineering, Beijing Jiaotong University, Beijing 100044, China (e-mail: hli@bjtu.edu.cn; 16121585@bjtu.edu.cn; 16121521@bjtu.edu.cn; tqzheng@bjtu.edu.cn; xjyou@bjtu.edu.cn).

K. Sun is with the Department of Electrical Engineering, Tsinghua University, Beijing 100084, China (e-mail: sun-kai@mail.tsinghua.edu.cn).

Color versions of one or more of the figures in this paper are available online at http://ieeexplore.ieee.org.

Digital Object Identifier 10.1109/TIE.2017.2721885

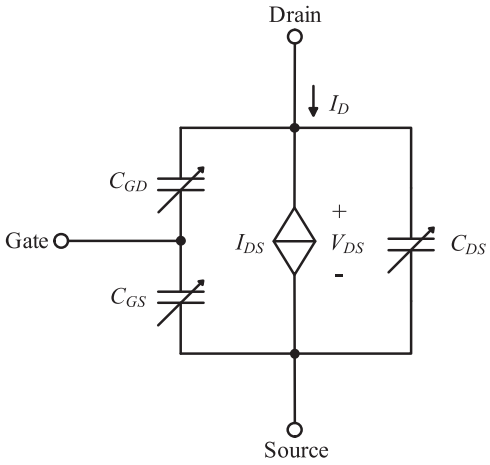

Fig. 1. Nonsegmented model of GaN HEMT.

problem in practice [17]. In order to improve the simulation convergence, this paper proposes a new behavioral model which uses nonsegmented, smooth continuous equations to describe the static and dynamic characteristics of GaN HEMT.

This paper chooses EPC 2010 (200 V/12 A) of enhancement mode GaN HEMT (eGaN HEMT) as modeling object, so all the GaN HEMTs mentioned below represent the EPC2010 of eGaN HEMT [18]. In Section II, the modeling process of the proposed GaN HEMT model and the parameter extraction are introduced in detail. In Section III, the nonsegmented model of GaN HEMT is verified by simulation and experiment to show the accuracy of the model. Furthermore, the proposed and conventional models are put into the full-bridge dc–ac converter to verify the good simulation convergence of the proposed model. Section IV summarizes the whole work of this paper.

II. Establishment of Nonsegmented Model

Nonsegmented model of GaN HEMT is shown in Fig. 1. This model includes voltage-dependent current source $I_{\rm DS}$ and voltage-dependent capacitances: gate–drain capacitance $C_{\rm GD}$, gate–source capacitance $C_{\rm GS}$, and drain–source capacitance $C_{\rm DS}$. The voltage-dependent current source $I_{\rm DS}$ is used to describe the static characteristic of GaN HEMT. Three voltage-dependent capacitances are used to describe the dynamic characteristic of GaN HEMT.

A. Nonsegmented Static Characteristic Model

The voltage-dependent current source $I_{\rm DS}$ describes the static *I–V* characteristic of GaN HEMT.

At present, $I_{\rm DS}$ is mostly divided into the cutoff region, linear region, and saturation region in the GaN HEMT model. From this method, it is difficult to determine the accurate boundary drain–source voltage $V_{\rm DS}$ between linear region and saturation region, and dividing $I_{\rm DS}$ into several segments may cause convergence problems when the model is applied into the power electronics circuit simulations. Based on this, this paper uses nonsegmented, smooth continuous equations to define $I_{\rm DS}$.

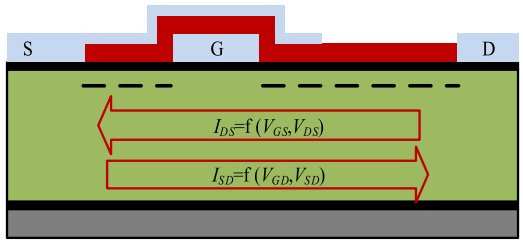

Fig. 2. Internal structure of GaN HEMT.

The internal structure of GaN HEMT is shown in Fig. 2 [19]. According to its working principle, the voltage-dependent current source $I_{\rm DS}$ mainly includes the transfer characteristic equation with the gate–source voltage $V_{\rm GS}$ as the variable, the output characteristic equation with the drain–source voltage $V_{\rm DS}$ as the variable, and the temperature characteristic equation with the temperature T as the variable.

In contrast to the vertical conduction channel of Si MOSFET, GaN HEMT has a nearly symmetrical transversal conduction channel. Therefore, the equation of reverse current $I_{\rm SD}$ is approximately the same as the forward current $I_{\rm DS}$, but the control voltages at the reverse conduction are the gate–drain voltage $V_{\rm GD}$ and the source–drain voltage $V_{\rm SD}$, so this paper will use the forward current $I_{\rm DS}$ as an example to introduce the modeling process of nonsegmented static characteristic model.

The equation of the transfer characteristic is based on the Motorola Electric Thermal model in the empirical model [20]; the specific equation is shown as follows:

$$I_{\rm DS} = A_1 \cdot \ln\left[1+\exp\left(\frac{V_{\rm GS}-b_1}{c_1}\right)\right] \tag{1}$$

where A_1, b_1, and c_1 are related parameters of the transfer characteristic.

The output characteristic equation is shown as follows:

$$I_{\rm DS} = A_2 \cdot \frac{V_{\rm DS}}{1+A_3 \cdot V_{\rm DS}} \tag{2}$$

where A_2 and A_3 are related parameters of the output characteristic.

According to the static characteristic curves provided in the datasheet, it can be found that the output characteristic displays different curves under different gate–source voltages $V_{\rm GS}$, so the gate–source voltage should be added as the variable in the output characteristic equation. And then the equation of the forward current $I_{\rm DS}$ at 25 °C can be obtained as follows:

$$I_{\rm DS} = K_1 \cdot \ln\left[1+\exp\left(\frac{V_{\rm GS}-b_1}{c_1}\right)\right] \cdot \frac{(m_1+n_1\cdot V_{\rm GS})\cdot V_{\rm DS}}{1+(d_1+e_1\cdot V_{\rm GS})\cdot V_{\rm DS}}, V_{\rm DS}>0 \tag{3}$$

where K_1, m_1, n_1, d_1, and e_1 are gate–source voltage related parameters of the output characteristic.

It should be noted that in the reverse conduction, the control voltage is the gate–drain voltage $V_{\rm GD}$, while

$$V_{\rm GD} = V_{\rm GS} + V_{\rm SD}. \tag{4}$$

10

Turkan Karakaya

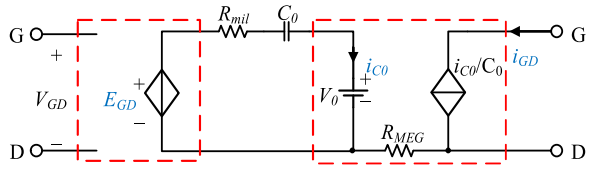

Fig. 3. Inherent capacitance modeling process.

When the source–drain voltage V_{SD} increases, gate–drain voltage V_{GD} also increases, which makes the reverse current I_{SD} to increase, that is, GaN HEMT has been working in the linear region in the reverse conduction. Therefore, the equation of reverse current I_{SD} can be simplified accordingly as follows:

11 urkan Karakaya

$$I_{DS} = -K_2 \cdot \ln\left[1+\exp\left(\frac{V_{GD}-b_2}{c_2}\right)\right]\cdot\frac{V_{SD}}{1+V_{SD}},\ V_{DS}\le 0 \tag{5}$$

where K_2, b_2, and c_2 are related parameters of the reverse conduction characteristic.

According to the datasheet, it can be found that the trend of the curves at different temperatures is basically the same, but the values of current are different [21], [22]. To ensure the simplification of the nonsegmented model, the final static model equation with temperature consideration is shown as follows:

12 urkan Karakaya

$$\begin{cases} I_{DS} = K_1(T)\cdot\ln\left[1+\exp\left(\frac{V_{GS}-b_1}{c_1}\right)\right] \\ \quad\cdot\frac{(m_1+n_1\cdot V_{GS})V_{DS}}{1+P_1(T)\cdot(d_1+e_1\cdot V_{GS})V_{DS}},\ V_{DS}>0 \\ I_{DS} = -K_2(T)\cdot\ln\left[1+\exp\left(\frac{V_{GD}-b_2}{c_2}\right)\right] \\ \quad\cdot\frac{V_{SD}}{1+P_1(T)\cdot V_{SD}},\qquad V_{DS}\le 0 \end{cases} \tag{6}$$

13 12.10.2017 urkan Karakaya

Among them are

14 urkan Karakaya

$$\begin{cases} K_1(T) = K_1\cdot\left[1-l_1\cdot(T-25)\right] \\ K_2(T) = K_2\cdot\left[1-l_2\cdot(T-25)\right] \\ P_1(T) = \left[1-h_1\cdot(T-25)\right] \\ P_2(T) = \left[1-h_2\cdot(T-25)\right] \end{cases} \tag{7}$$

where l_1, l_2, h_1, and h_2 are related parameters of the temperature characteristic.

B. Nonsegmented Dynamic Characteristic Model

The dynamic characteristic of GaN HEMT is mainly determined by three inherent capacitances. According to the capacitance–voltage (C–V) characteristic curves provided in the datasheet, the gate–source capacitance C_{GS}, the gate–drain capacitance C_{GD}, and drain–source capacitance C_{DS} can be described by the voltage-dependent nonlinear equations. Taking gate–drain capacitance C_{GD} as an example, i_{GD} is the equivalent current to describe the capacitance C_{GD}. Fig. 3 shows the modeling process of inherent capacitance in this paper.

15-16 2 notes:

The constant linear capacitance C_0 can generate current i_{C0} varying with the voltage V_{GD} by means of the voltage-dependent voltage source E_{GD}, then we can get the equivalent current i_{GD} by means of the current-dependent current source to describe the nonlinear capacitance [23]–[25]. The differential characteristic of the capacitance C_{GD} is realized by the linear capacitance C_0, which greatly simplifies the simulation. The modeling principle is shown as follows:

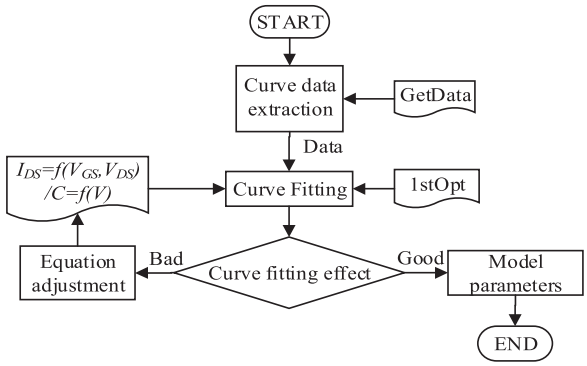

Fig. 4. Parameter extraction method.

$$\begin{aligned} E_{GD} = f(V_{GD}) \Rightarrow i_{C_0} &= C_0\frac{dE_{GD}}{dt} \\ \Rightarrow i_{GD} &= \frac{1}{C_0}i_{C_0} \Rightarrow i_{GD} \approx C_{GD}. \end{aligned} \tag{8}$$

In the capacitance model, we need to get the equation of E_{GD} and i_{GD}. According to the C–V characteristic curves, the equation of i_{GD} can be obtained by data extraction and fitting, and i_{GD} and E_{GD} have differential relationship, which is shown as follows:

$$E_{GD} = \int i_{GD}\,dt. \tag{9}$$

Based on these, the equations of i_{GD} and E_{GD} can be obtained as follows:

$$\begin{cases} i_{GD} = s\cdot\frac{1}{1+\exp\left(\frac{p-V_{GD}}{q}\right)}+r \\ E_{GD} = s\cdot q\cdot\ln\left[1+\exp\left(\frac{V_{GD}-p}{q}\right)\right]+r\cdot V_{GD} \end{cases} \tag{10}$$

where s, p, q, and r are related parameters of the capacitance–voltage characteristic.

C. Model Parameters Extraction

The static characteristic I–V curves and dynamic characteristic C–V curves required for model parameters extraction are provided by GaN HEMT datasheet. The parameter extraction method is shown in Fig. 4.

First of all, curve information provided in datasheet is converted to the data information required for parameter extraction with the help of data extraction software GetData. And then we can use the data and the I–V, C–V equations to do the curve fitting in software 1stOpt [6]. According to the results shown in 1stOpt, we can do some corresponding adjustments to the equations to obtain the accurate model parameters [26].

The static model parameters at 25 °C are shown in Table I.

The parameters related to the temperature are shown in Table II.

For the capacitance parameters, the datasheet only provides the transfer capacitance C_{rss}, input capacitance C_{iss}, and output

TABLE I
STATIC MODEL PARAMETERS AT 25 °C

Parameter	K_1	b_1	c_1	d_1	e_1
Value	0.283	2.035	0.124	1.159	−0.204
Parameter	m_1	n_1	K_2	b_2	c_2
Value	30.972	−4.48	7.114	2.054	0.153

TABLE II
TEMPERATURE PARAMETERS OF STATIC MODEL

Parameter	l_1	h_1	l_2	h_2
Value	4.316e−3	3.771e−3	−1.091e−3	−7.872e−3

TABLE III
CAPACITANCE PARAMETERS

Parameter	s	p	q	r
C_{GD}	0.1004	−4.643	5.032	9.48e−3
C_{DS}	0.49	−13.263	1.844	0.229
C_{GS}	−0.067	6.733	5.39	0.469

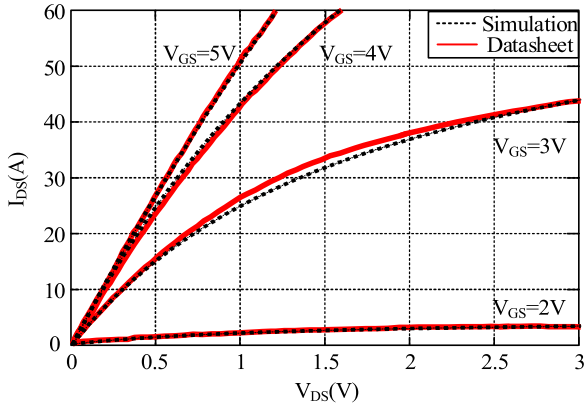

Fig. 5. Forward output characteristic comparison between simulation (dashed line) and datasheet (solid line).

capacitance C_{oss} curves, but we can obtain the desired capacitance data with the equation shown as follows:

17

Melisa SARICI

$$\begin{cases} C_{GD} = C_{rss} \\ C_{GS} = C_{iss} - C_{rss} \\ C_{DS} = C_{oss} - C_{rss} \end{cases}. \tag{11}$$

The extracted capacitance parameters are shown in Table III.

III. VERIFICATION OF THE NONSEGMENTED MODEL

The verification of the nonsegmented model includes the static characteristic, the dynamic characteristic, and the simulation convergence. Each part is described in more details below.

A. Verification of Static Characteristic

The verification of the static characteristic is comparing the simulation curves with datasheet curves, and the static characteristic curves provided in datasheet include the forward output characteristic at 25 °C, and the forward transfer characteristic and reverse output characteristic at 25 °C and 125 °C.

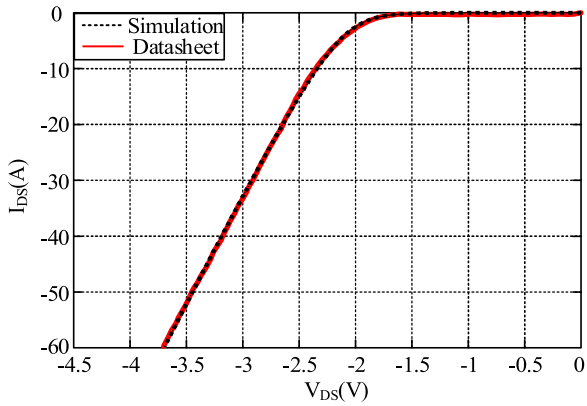

Fig. 6. Reverse output characteristic comparison between simulation (dashed line) and datasheet (solid line).

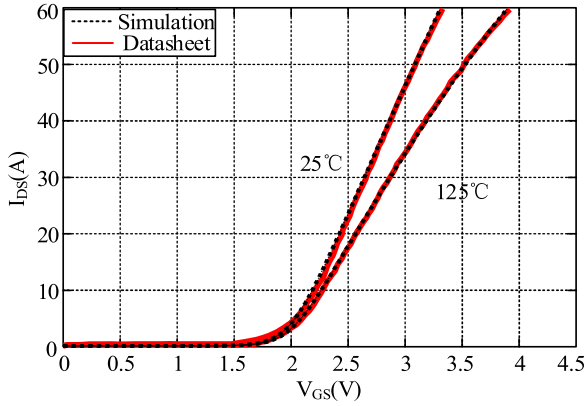

Fig. 7. Forward transfer characteristic comparison between simulation (dashed line) and datasheet (solid line) at 25 °C and 125 °C.

According to the parameters presented in Table I, the static model can be built in PSpice, and then the curves can be obtained with the dc sweep analysis. Figs. 5 and 6 show the comparisons between simulation (dashed lines) curves and datasheet (solid lines) curves, in forward and reverse conduction modes, respectively. The simulation curves are in good agreement with datasheet curves.

According to the parameters in Table II, the temperature-dependent static model can be built in PSpice, and the reverse output characteristic and forward transfer characteristic curves at different temperatures can be obtained with the temperature sweep analysis in PSpice. Figs. 7 and 8 show the comparisons between simulation (dashed lines) curves and datasheet (solid lines) curves under temperatures 25 °C and 125 °C, in forward transfer and reverse output modes, respectively. The simulation curves are in good agreement with datasheet curves at 25 °C and 125 °C.

B. Verification of Dynamic Characteristic

The inherent capacitance determines the dynamic characteristic of GaN HEMT, so the inherent capacitance model needs to be verified by comparing the simulation curves with

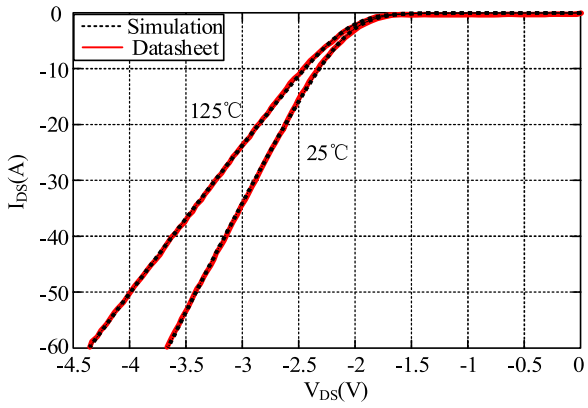

Fig. 8. Reverse output characteristic comparison between simulation (dashed line) and datasheet (solid line) at 25 °C and 125 °C.

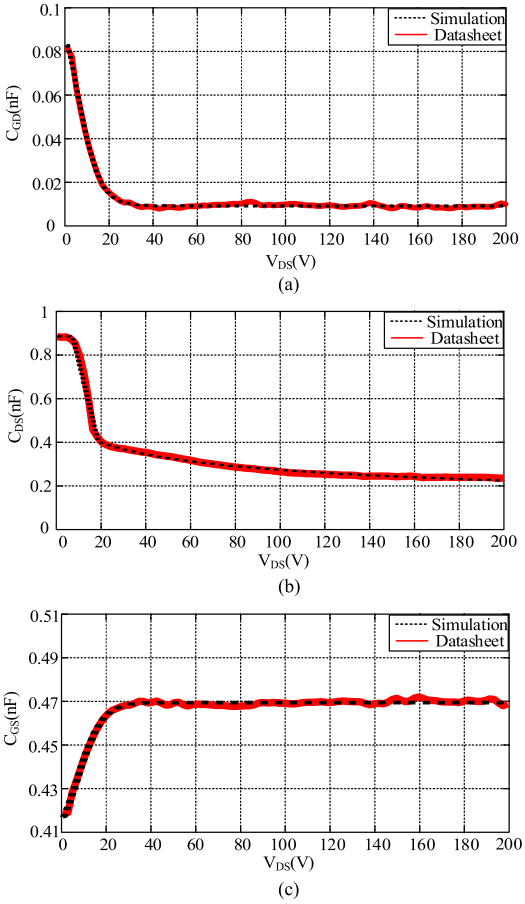

Fig. 9. Comparison between simulation (dashed line) and datasheet (solid line). (a) Gate–drain capacitance; (b) drain–source capacitance; and (c) gate–source capacitance.

datasheet curves. The simulation curves can be obtained with the time domain transient in PSpice. Fig. 9 shows the gate–drain, drain–source, and gate–source capacitance comparisons between simulation (dashed lines) and datasheet (solid lines). The simulation curves are in good agreement with datasheet curves.

In addition, the dynamic characteristic also includes the voltage and current changes of GaN HEMT under switching condition. In order to verify whether the dynamic characteristic

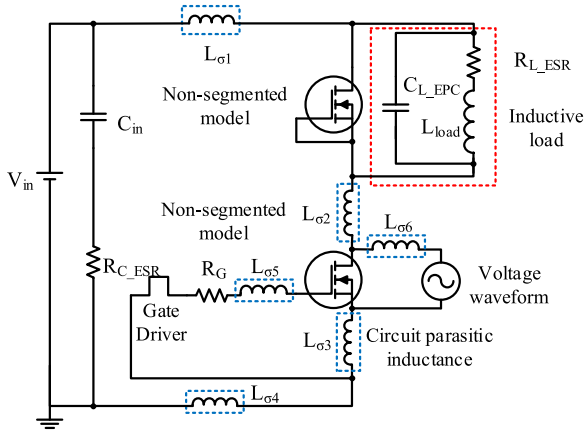

Fig. 10. Double pulse simulation circuit.

TABLE IV
PARAMETERS OF STRAY INDUCTANCE

Parameter	$L_{\sigma 1}$	$L_{\sigma 2}$	$L_{\sigma 3}$	$L_{\sigma 4}$	$L_{\sigma 5}$	$L_{\sigma 6}$
Value (nH)	8	7	2	10	2	5

TABLE V
PARAMETERS OF DOUBLE PULSE CIRCUIT

Parameter	Input Voltage V_{in} (V)	Load Current (A)	Inductive load L_{load} (μH)	Gate resistance R_G (Ω)
Value	95	5.72	220	2.7

of the nonsegmented model under switching condition is correct, a double pulse test platform is built [27], [28]. The double pulse test circuit has a phase leg structure with GaN HEMT EPC 2010 pairs; this structure makes the voltage and current waveforms of the low-side EPC to reflect the forward and reverse dynamic characteristics of GaN HEMT. The gate driver is LM5114 from Texas Instruments, which is designed to drive low-side enhancement mode GaN HEMTs. The high-side GaN HEMT in the double pulse circuit is always in the off-state, so shorting its gate and source directly. The experiment is done with an inductive load at room temperature.

The double pulse simulation circuit in PSpice is shown in Fig. 10. The parasitic parameters are also taken into account during simulation to predict the voltage and current transient spikes, ringing, and shocks [29], [30]. The parasitic parameters of inductor and capacitor are obtained by *RLC* meter Fluke PM6306. According to the actual double pulse circuit printed circuit board (PCB) layout and welding conditions, the stray inductances should be added into the circuit too [31]. The stray inductances in the circuit are extracted by Ansoft Q3D, and the extracted stray inductance parameters are shown in Table IV. The double pulse circuit parameters are shown in Table V.

The voltage and current simulation waveforms of low-side GaN HEMT are shown in Fig. 11.

Instrument types and parameters used in the double pulse experiment are shown in Table VI. The double pulse test platform is shown in Fig. 12. The parameters of the circuit are the same

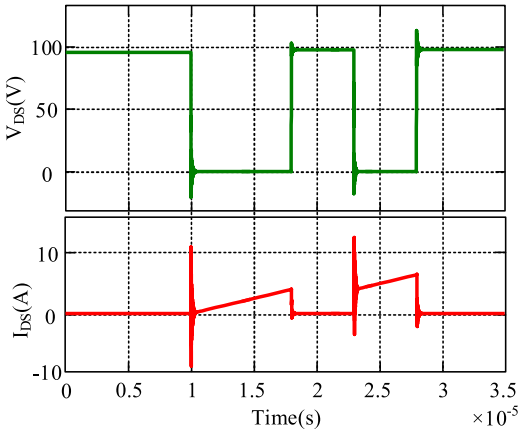

Fig. 11. Simulation waveforms of double pulse circuit.

TABLE VI
EXPERIMENT INSTRUMENT TYPES AND PARAMETERS

Instrument	Type	Parameter
DC power supply	*Chroma 62050P*	0–600 V
Oscilloscope	*Tektronix DPO4054B*	500 MHz
Voltage probe	Tektronix P220	200 MHz/600 V
Current probe	Tektronix TCP0030	120 MHz/30 A
DSP control board	TMS320F28335	

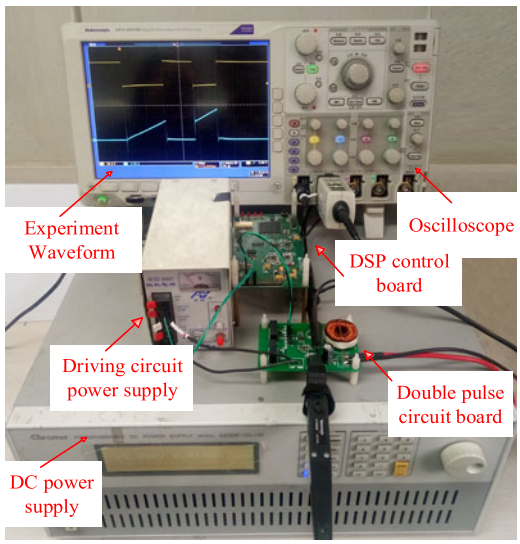

Fig. 12. Double pulse circuit test platform.

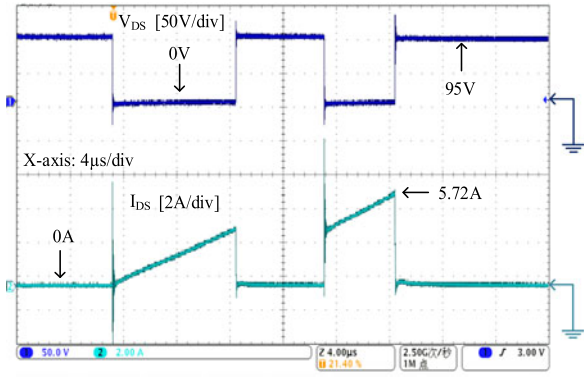

Fig. 13. Experimental waveforms of double pulse circuit.

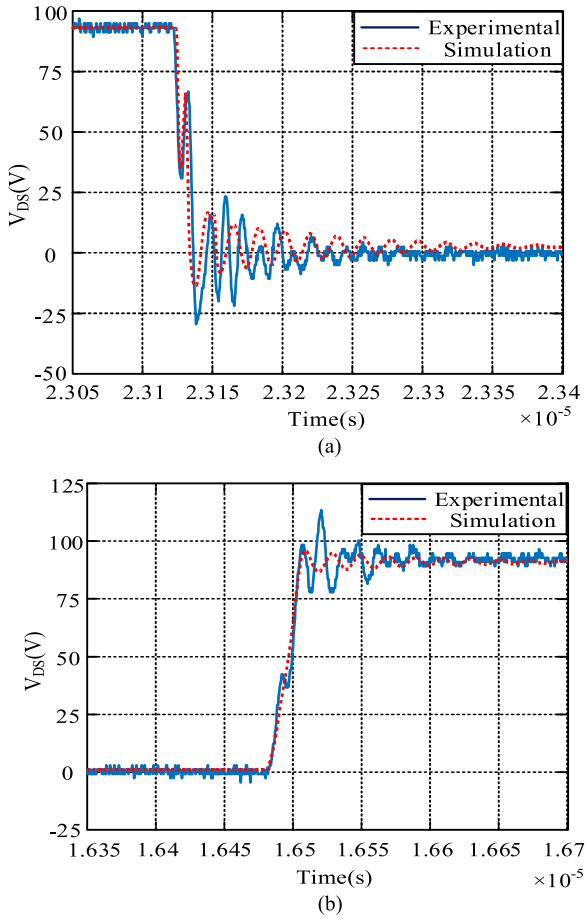

Fig. 14. Voltage waveforms comparison between simulation (dashed line) and experimental (solid line). (a) Turn-ON transient and (b) turn-OFF transient.

as those in the simulation. The low-side GaN HEMT voltage and current experiment waveforms are shown in Fig. 13.

Figs. 14 and 15 show the comparisons of simulation (dashed lines) and experimental (solid lines) voltage and current waveforms during turn-ON and turn-OFF transient. The value of rise time and fall time of the simulation and experiment is shown in Table VII.

Comparison results show that the simulation waveforms and experimental waveforms can basically match, but the stray parameters of the circuit cannot be fully considered, so the two waveforms still have some differences. On the whole, the simulation waveforms can accurately reflect the voltage and current changes of GaN HEMT under switching condition.

C. Verification of Simulation Convergence

In order to verify the simulation convergence of proposed GaN HEMT nonsegmented model, the proposed model and the conventional model are employed into the same full-bridge dc–ac converter. The conventional segmented GaN HEMT model in [15] is taken as example, the unipolar sinusoidal pulse width

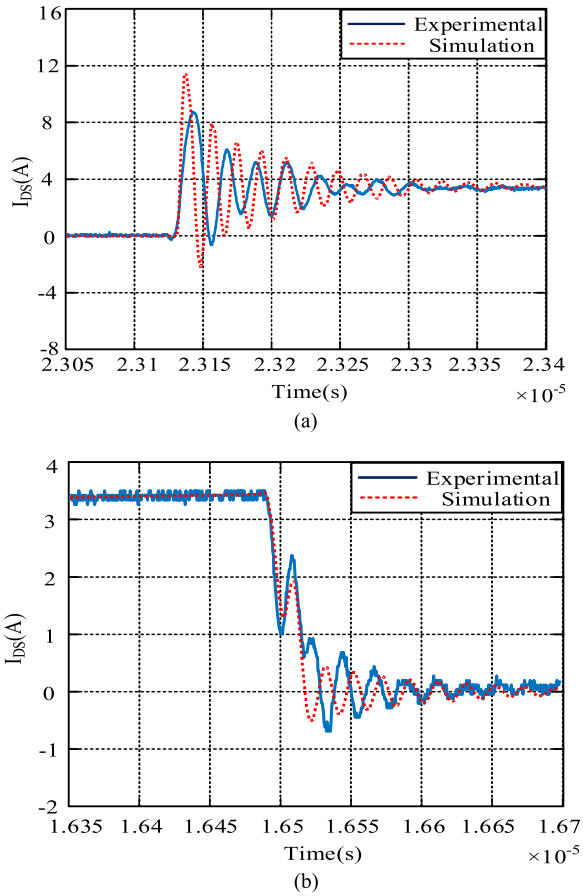

Fig. 15. Current waveforms comparison between simulation (dashed line) and experimental (solid line). (a) Turn-ON transient and (b) turn-OFF transient.

TABLE VII
SIMULATION AND EXPERIMENT COMPARISON OF RISE TIME AND FALL TIME

Parameter	Rise time		Fall time	
	Voltage rise time t_{rv} (ns)	Current rise time t_{ri} (ns)	Voltage fall time t_{fv} (ns)	Current fall time t_{fi} (ns)
Simulation	15.91	3.38	10.22	21.563
Experiment	16.4	3.53	12.24	32.72
Error (%)	2.99	4.25	16.5	34.1

modulation (SPWM) is used for the full-bridge dc–ac converter, and the inverter topology and the drive signals under unipolar SPWM are shown in Figs. 16 and 17. The simulation circuit parameters are shown in Table VIII.

Fig. 18(a) shows that the full-bridge dc–ac converter under unipolar SPWM can be simulated well using the proposed nonsegmented model and the waveforms of the bridge arm midpoints voltage $V_{\rm out}$ and the load voltage V_R are both correct, however, the simulation of this inverter with the conventional segmented model cannot converge, as shown in Fig. 18(b).

In order to further compare the simulation convergence of these two models, the inductor L and capacitor C in Fig. 16 are removed, and simulating the inverter with these two models again, the simulation results are shown in Fig. 19.

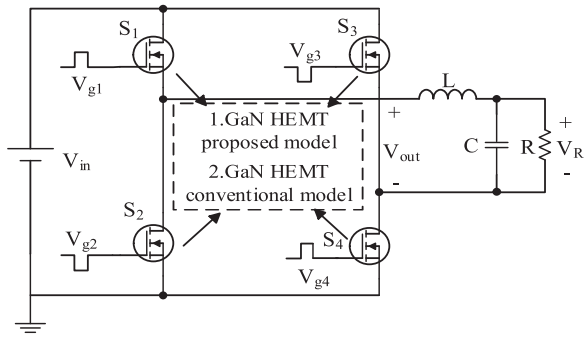

Fig. 16. Topology of full-bridge dc–ac converter.

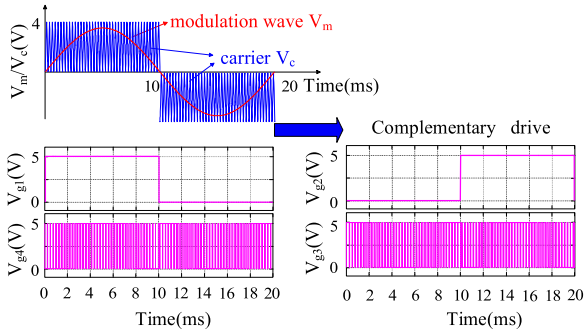

Fig. 17. Dive signals for S_1–S_4 under unipolar SPWM.

TABLE VIII
SIMULATION PARAMETERS OF A FULL-BRIDGE INVERTER

Parameter	Input voltage V_{in} (V)	Inductance L (mH)	Capacitance C (μF)	Resistance R (Ω)
Value	100	2	230	5.3

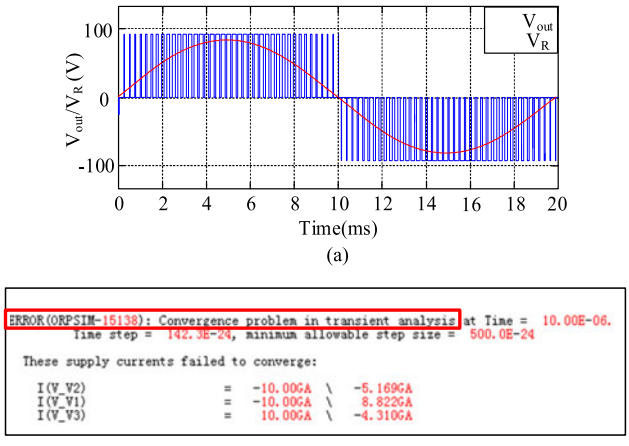

Fig. 18. Simulation results of the full-bridge dc–ac inverter (a) with proposed nonsegmented model and (b) with conventional segmented model.

Fig. 19 shows that the waveform of $V_{\rm out}$ with proposed nonsegmented model is correct. However, with the conventional segmented GaN HEMT model in [15], the simulation waveform of $V_{\rm out}$ is seriously distorted. Therefore, the proposed nonsegmented GaN HEMT model is helpful to improve the simulation

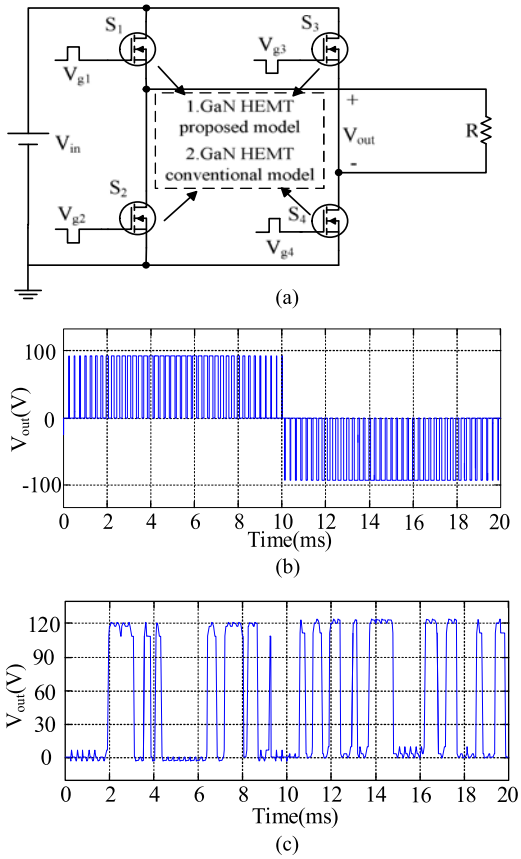

Fig. 19. Simplified inverter and the simulation results of $V_{\rm out}$ with two different models: (a) the simplified full-bridge dc–ac inverter (b) with the proposed nonsegmented model and (c) with conventional segmented model.

convergence and the simulation correctness effectively, and it is good for practical circuits simulation.

IV. Conclusion

In this paper, a nonsegmented PSpice circuit model of GaN HEMT was proposed. The static and dynamic characteristics of the proposed nonsegmented model were well verified based on the datasheet and double pulse platform. Furthermore, the proposed model of GaN HEMT was first applied into the real power electronics circuit simulation in this paper, and the good simulation convergence of the proposed nonsegmented PSpice circuit model was also proved by the simulation results of a full-bridge dc–ac converter compared to the conventional segmented GaN HEMT model. Therefore, the proposed nonsegmented PSpice circuit model of GaN HEMT made the design and analysis of power converters with GaN HEMTs more convenient and efficient.

References

[1] J. Millan, P. Godignon, X. Perpina, A. Perez-Tomas, and J. Rebollo, "A survey of wide bandgap power semiconductor devices," *IEEE Trans. Power Electron.*, vol. 29, no. 5, pp. 2155–2163, May 2014.

[2] M. Rodríguez, Y. Zhang, and D. Maksimović, "High-frequency PWM buck converters using GaN-on-SiC HEMTs," *IEEE Trans. Power Electron.*, vol. 29, no. 5, pp. 2462–2473, May 2014.

[3] G. C. Barisich, A. Ç. Ulusoy, E. Gebara, and J. Papapolymerou, "A reactively matched 1.0–11.5 GHz hybrid packaged GaN high power amplifier," *IEEE Microw. Wireless Compon. Lett.*, vol. 25, no. 12, pp. 811–813, Dec. 2015.

[4] Z. L. Zhang, Z. Dong, D. D. Hu, X. W. Zou, and X. Ren, "Three-level gate drivers for eGaN HEMTs in resonant converters," *IEEE Trans. Power Electron.*, vol. 32, no. 7, pp. 5527–5538, Jul. 2017.

[5] K. Wang, X. Yang, H. Li, H. Ma, X. Zeng, and W. Chen, "An analytical switching process model of low-voltage eGaN HEMTs for loss calculation," *IEEE Trans. Power Electron.*, vol. 31, no. 1, pp. 635–647, Jan. 2016.

[6] Y. M. Xu, H. Li, T. Q. Zheng, B. Zhao, and Z. Zhou, "Study on the PSpice simulation model of SiC MOSFET base on its datasheet," in *Proc. IEEE Int. Future Energy Electron. Conf.*, Nov. 2015, pp. 1–6.

[7] H. A. Mantooth, K. Peng, E. Santi, and J. L. Hudgins, "Modeling of wide bandgap power semiconductor devices—Part I," *IEEE Trans. Electron Devices*, vol. 62, no. 2, pp. 423–433, Feb. 2015.

[8] E. Santi, K. Peng, H. A. Mantooth, and J. L. Hudgins, "Modeling of wide-bandgap power semiconductor devices—Part II," *IEEE Trans. Electron Devices*, vol. 62, no. 2, pp. 434–442, Feb. 2015.

[9] H. L. Huang, Y. C. Liang, and G. S. Samudra, "Theoretical calculation and efficient simulations of power semiconductor AlGaN/GaN HEMTs," in *Proc. IEEE Int. Conf. Electron Devices Solid State Circuit*, Dec. 2012, pp. 1–4.

[10] S. Strauss, A. Erlebach, T. Cilento, D. Marcon, S. Stoffels, and B. Bakeroot, "TCAD methodology for simulation of GaN-HEMT power devices," in *Proc. IEEE Int. Symp. Power Semicond. Devices ICs*, Jun. 2014, pp. 257–260.

[11] B. Syamal, X. Zhou, S. B. Chiah, A. M. Jesudas, S. Arulkumaran, and G. I. Ng, "A comprehensive compact model for GaN HEMTs, including quasi-steady-state and transient trap-charge effects," *IEEE Trans. Electron Devices*, vol. 63, no. 4, pp. 1478–1485, Apr. 2016.

[12] J. Waldron and T. P. Chow, "Physics-based analytical model for high-voltage bidirectional GaN transistors using lateral GaN power HEMT," in *Proc. IEEE Int. Symp. Power Semicond. Devices ICs*, May 2013, pp. 213–216.

[13] K. Shah and K. Shenai, "Simple and accurate circuit simulation model for gallium nitride power transistors," *IEEE Trans. Electron Devices*, vol. 59, no. 10, pp. 2735–2742, Oct. 2012.

[14] G. H. Aghdam, "Model characterization and performance evaluation of GaN FET in DC-DC POL regulators," in *Proc. IEEE Int. Telecommun. Energy Conf.*, Oct. 2015, pp. 1–4.

[15] K. Peng, S. Eskandari, and E. Santi, "Characterization and modeling of a gallium nitride power HEMT," *IEEE Trans. Ind. Appl.*, vol. 52, no. 6, pp. 4965–4975, Nov./Dec. 2016.

[16] R. Xie, H. Wang, G. Tang, X. Yang, and K. J. Chen, "An analytical model for false turn-on evaluation of GaN transistor in bridge-leg configuration," in *Proc. IEEE Energy Convers. Congr. Expo.*, Sep. 2016, pp. 1–6.

[17] L. Zheng, J. Tian, Z. Weng, H. Hu, J. Wu, and W. Sun, "An improved convergent model for single-photon avalanche diodes," *IEEE Photon. Technol. Lett.*, vol. 29, no. 10, pp. 798–801, May 2017.

[18] Efficient Power Conversion Corporation, "EPC 2010_datasheet," Feb. 2013. [Online]. Available: http://epc-co.com/epc/Portals/0/epc/documents/datasheets/epc2010_datasheet.pdf

[19] S. L. Colino and R. A. Beach, "Fundamentals of gallium nitride power transistors," 2009. [Online]. Available: http://epc-co.com/epc/Portals/0/epc/documents/product-training/Appnote_GaNfundamentals.pdf

[20] W. R. Curtice, "GaAs MESFET modeling and nonlinear CAD," *IEEE Trans. Microw. Theory Techn.*, vol. 36, no. 2, pp. 220–230, Feb. 1988.

[21] G. Crupi, A. Raffo, G. Avolio, D. M. M.-P. Schreurs, G. Vannini, and A. Caddemi, "Temperature influence on GaN HEMT equivalent circuit," *IEEE Microw. Wireless Compon. Lett.*, vol. 26, no. 10, pp. 813–815, Oct. 2016.

[22] H. Sun *et al.*, "Temperature-dependent thermal resistance of GaN-on-diamond HEMT wafers," *IEEE Electron Device Lett.*, vol. 37, no. 5, pp. 621–624, May 2016.

[23] J. Q. Wu and H. Y. Li, "Construction of nonlinear capacitance PSpice model," *J. Harbin Inst. Technol.*, vol. 3, pp. 44–46, Jun. 1999.

[24] G. Crupi *et al.*, "High-frequency extraction of the extrinsic capacitances for GaN HEMT technology," *IEEE Microw. Wireless Compon. Lett.*, vol. 21, no. 8, pp. 445–447, Aug. 2011.

[25] S. Aamir Ahsan, S. Ghosh, K. Sharma, A. Dasgupta, S. Khandelwal, and Y. S. Chauhan, "Capacitance modeling in dual field-plate power GaN HEMT for accurate switching behavior," *IEEE Trans. Electron Devices*, vol. 63, no. 2, pp. 565–572, Feb. 2016.
[26] A. Jarndal, R. Essaadali, and A. B. Kouki, "A reliable model parameter extraction method applied to AlGaN/GaN HEMTs," *IEEE Trans. Comput.-Aided Des. Integr. Circuits Syst.*, vol. 35, no. 2, pp. 211–219, Feb. 2016.
[27] D. Reusch and J. Strydom, "Understanding the effect of PCB layout on circuit performance in a high-frequency gallium-nitride-based point of load converter," *IEEE Trans. Power Electron.*, vol. 29, no. 4, pp. 2008–2015, Apr. 2014.
[28] J. Wang, H. S. H. Chung, and R. T. H. Li, "Characterization and experimental assessment of the effects of parasitic elements on the MOSFET switching performance," *IEEE Trans. Power Electron.*, vol. 28, no. 1, pp. 573–590, Jan. 2013.
[29] R. Fu, A. Grekov, K. Peng, and E. Santi, "Parasitic modeling for accurate inductive switching simulation of converters using SiC Devices," in *Proc. IEEE Energy Convers. Congr. Expo.*, Sep. 2013, pp. 1259–1265.
[30] Z. Liu, X. Huang, F. C. Lee, and Q. Li, "Package parasitic inductance extraction and simulation model development for the high-voltage cascode GaN HEMT," *IEEE Trans. Power Electron.*, vol. 29, no. 4, pp. 1977–1985, Apr. 2014.
[31] K. Sun, J. J. Lu, H. F. Wu, Y. Xing, and L. P. Huang, "Solving temperature parameter modeling of silicon carbide MOSFET," *J. Chin. Electr. Eng. Sci.*, vol. 33, no. 3, pp. 37–43, Jan. 2013.

Hong Li (S'07–M'09) received the B.Sc. degree in electrical engineering from Taiyuan University of Technology, Taiyuan, China, in 2002, the M.Sc. degree in electrical engineering from South China University of Technology, Guangzhou, China, in 2005, and the Ph.D. degree in electrical engineering from Fernuniversität, Hagen, Germany, in 2009.

Currently, she is a Professor with the Electrical Engineering School, Beijing Jiaotong University, Beijing, China. She has published 1 book, 25 journal papers, and 38 conference papers. She has also applied 20 patents. Her research interests include nonlinear modeling, analysis and its applications, EMI suppressing methods for power electronic system, wide-bandgap power devices, and applications.

Dr. Li is an associate editor for the *Chinese Journal of Electrical Engineering* and the Vice Chairman of Electromagnetic Compatibility Specialized Committee in China Power Supply Society.

Xingran Zhao was born in Hebei Province, China, in 1994. She received the B.S. degree in electrical engineering from Beijing Jiaotong University, Beijing, China, in 2016, where she is currently working toward the M.S. degree in electrical engineering.

Her research interests include the modeling and application of wide-bandgap power devices.

Wenzhe Su was born in Shanxi Province, China, in 1993. He received the B.S. degree in electrical engineering from Shanxi University, Shanxi, China, in 2016.

His research interests include the application of power electronics in power systems and renewable energy power generation.

Kai Sun (M'12–SM'16) received the B.E., M.E., and Ph.D. degrees in electrical engineering from Tsinghua University, Beijing, China, in 2000, 2002, and 2006, respectively.

In 2006, he joined the Faculty of Electrical Engineering, Tsinghua University, where he is currently an Associate Professor. From September 2009 to August 2010, he was a Visiting Scholar with the Department of Energy Technology, Aalborg University, Aalborg, Denmark. From January to August 2017, he was a Visiting Professor with the Department of Electrical and Computer Engineering, University of Alberta, Edmonton, AB, Canada. His current research interests include power electronics for renewable generation systems, microgrids, and active distribution networks.

Dr. Sun is a member of the IEEE Power Electronics Society Sustainable Energy Systems Technical Committee, the IEEE Power Electronics Society Power and Control Core Technologies Committee, the IEEE Industrial Electronics Society Renewable Energy Systems Technical Committee, and the IEEE Industry Applications Society Industrial Drive Committee Awards Sub-committee. He is an associate editor for the *Journal of Power Electronics*. He was the recipient of the Delta Young Scholar Award in 2013.

Trillion Q. Zheng (M'06–SM'07) was born in Jiangshan, Zhejiang, China, in 1964. He received the B.S. degree from Southwest Jiaotong University, Sichuan, China, in 1986, and the M.S. and Ph.D. degrees from Beijing Jiaotong University, Beijing, China, in 1992 and 2002, respectively, all in electrical engineering.

He is currently a University Distinguished Professor with Beijing Jiaotong University. He directs the Center for Electric Traction, founded by the Ministry of Education, China. From 2003 to 2011, he served as the Dean in the School of Electrical Engineering, Beijing Jiaotong University. He holds 17 Chinese patents and has published more than 60 journal articles and more than 100 technical papers in conference proceedings. His research interests include power supply and ac drive of railway traction systems, high performance and low loss for power electronics systems, PV-based converters and control, and active power filter and power quality correction.

Dr. Zheng is currently the Deputy Director of the Council of Beijing Society for Power Electronics and a member of the Council of China Electrotechnical Society. He received the Excellent Teacher Award of Beijing Government in 1997, and the Youth Award of Railway Science and Technology of Zhan Tianyou in 2005. He was Laureates of Youth Elite of Science and Technology, Railway Ministry of China in 1998 and of Zhongda Scholar for power electronics and motor drive area, by Delta Environmental and Educational Foundation in 2007.

Xiaojie You was born in Fujian Province, China, in 1964. He received the M.S. degree from China Agricultural University, Beijing, China, in 1989, and the Ph.D. degree from Czech Technical University, Prague, Czech Republic, in 2001, both in electrical engineering.

From 2002 to 2004, he was a Postdoctoral Research Fellow with Tsinghua University, Beijing, China. From 2004 to 2006, he was an Associate Professor with the School of Electrical Engineering, Beijing Jiaotong University, Beijing, China, where he has been a Professor and the Director of Power Electronic Research Institute since 2006. His current research interests include ac drive electric locomotive control, switching power control, active power filters, and power quality control.

Nonsegmented PSpice Circuit Model of GaN HEMT With Simulation Convergence Consideration

Li, Hong; Zhao, Xingran; Su, Wenzhe; Sun, Kai; You, Xiaojie; Zheng, Trillion Q

01 Furkan Karakaya Page 1

13/10/2017 7:32

GaN modellemesi üzerine çok faydalı olacak bir çalışma. Fiziksel modelleme yerine davranışsal modelleme önplana çıkarılmış ve modellemenin nasıl yapılacağı iyi bir şekilde anlatılmış.

02 Furkan Karakaya Page 1

12/10/2017 13:59

03 Furkan Karakaya Page 1

12/10/2017 13:59

04 Furkan Karakaya Page 1

12/10/2017 13:59

05 Furkan Karakaya Page 1

12/10/2017 13:59

06 Furkan Karakaya Page 1

12/10/2017 13:59

Power Electronic uygulamalarında modellemelerden hangisinin tercih edilmesi gerektiği hakkında iyi bir açıklama yapılmış.

07 Furkan Karakaya Page 1

12/10/2017 13:59

08 Furkan Karakaya Page 1

12/10/2017 13:59

09 Furkan Karakaya Page 1

12/10/2017 13:59

15-16 Mendeley'de var. Bu iki makalede anlatılan yöntemlerde segmented yaklaşım ile denklemler oluşturulmuştu, bu paper nonsegmented yaklaşım ile hazırlanmış.

10 Furkan Karakaya Page 2

12/10/2017 13:59

11 Furkan Karakaya Page 3

12/10/2017 13:59

12 Furkan Karakaya Page 3

18/10/2017 8:39

13 Furkan Karakaya Page 3

12/10/2017 13:59

Equationlar bunlar:

14 Furkan Karakaya Page 3

18/10/2017 8:39

15 Furkan Karakaya Page 3

13/10/2017 7:32

GetData bizim de datasheetteki grafikleri parametreleştirmemizde iyi olacaktır.

16 Furkan Karakaya Page 3

13/10/2017 7:32

17 Melisa SARICI Page 4

7/11/2017 19:49

18 Melisa SARICI Page 5

20/10/2017 11:15

19 Melisa SARICI Page 5

20/10/2017 11:15

20 Melisa SARICI Page 5

20/10/2017 11:15

21 Melisa SARICI Page 5

20/10/2017 11:15

22 Melisa SARICI Page 5

20/10/2017 11:15

23 Melisa SARICI Page 5

20/10/2017 11:15

24 Melisa SARICI Page 5

20/10/2017 11:15

25 Melisa SARICI Page 5

20/10/2017 11:15

26 Furkan Karakaya Page 5

13/10/2017 7:32

27 Melisa SARICI Page 5

20/10/2017 11:15

28 Furkan Karakaya Page 6

13/10/2017 7:32

Stray parametrelerindeki hatalardan dolayı grafikler tam oturmamış ama yine de sonuçlar uyumlu